

See discussions, stats, and author profiles for this publication at: <https://www.researchgate.net/publication/258684108>

# High Fracture Efficiency and Stress Concentration Phenomenon for Microgel-Reinforced Hydrogels Based on Double-Network Principle

ARTICLE *in* MACROMOLECULES · DECEMBER 2012

Impact Factor: 5.8 · DOI: 10.1021/ma301933x

---

CITATIONS

22

---

READS

53

## 8 AUTHORS, INCLUDING:



Tasuku Nakajima

Hokkaido University

37 PUBLICATIONS 523 CITATIONS

[SEE PROFILE](#)



Zi Liang Wu

Zhejiang University

29 PUBLICATIONS 459 CITATIONS

[SEE PROFILE](#)

## High Fracture Efficiency and Stress Concentration Phenomenon for Microgel-Reinforced Hydrogels Based on Double-Network Principle

Jian Hu,<sup>†</sup> Takayuki Kurokawa,<sup>‡,§</sup> Tasuku Nakajima,<sup>‡</sup> Tao Lin Sun,<sup>†</sup> Tiffany Suekama,<sup>†</sup> Zi Liang Wu,<sup>†</sup> Song Miao Liang,<sup>‡</sup> and Jian Ping Gong\*,<sup>‡,§</sup>

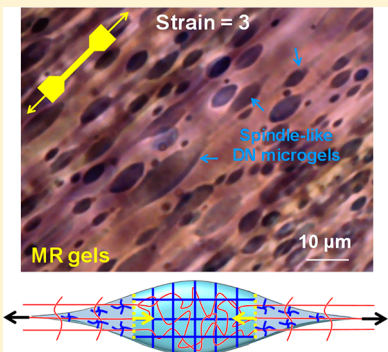
<sup>†</sup>Graduate School of Science, Hokkaido University, Sapporo 060-0810, Japan

<sup>‡</sup>Faculty of Advanced Life Science, Hokkaido University, Sapporo 060-0810, Japan

<sup>§</sup>Creative Research Initiative Sousei, Hokkaido University, Sapporo 001-0021, Japan

<sup>†</sup>Department of Chemical and Petroleum Engineering, University of Kansas, Lawrence, Kansas 66045, United States

**ABSTRACT:** Double-network hydrogels (DN gels) have aroused considerable interest because of their excellent mechanical strength and toughness, low sliding friction, good biocompatibility, as well as wide tunability in components. By revisiting DN gels, we provide an ingenious way to fabricate a kind of strong and tough microgel-reinforced hydrogels (MR gels), that densely cross-linked polyelectrolyte microgels of poly(2-acrylamido-2-methylpropanesulfonic sodium) (PNaAMPS) (replacing the densely cross-linked PNaAMPS macro-network for conventional DN gels) are incorporated into sparsely cross-linked neutral polyacrylamide (PAAm) matrix. The structure of MR gels can be considered as a two-phase composite, where the disperse phase is the *rigid* DN microgels, and the continuous phase is the *soft* PAAm matrix. Similar to DN gels, MR gels show the irreversible energy dissipation in the hysteresis measurement, demonstrating the permanent fracture of the brittle PNaAMPS phase. Thus, the discontinuous brittle phase also serves as *sacrificial bonds*. Through quantitative comparison of the hysteresis curves with DN gels and monitoring the morphology change of the embedded microgels in MR gels during the real-time stretching process, we conclude that the DN microgels in MR gels show four times higher in fracture efficiency of the *sacrificial bonds* than bulk DN gels at the same strain, as a result of the stress concentration around the microgels.



### INTRODUCTION

Hydrogel science and engineering is a field of important research today where the quest for the Holey Grail is clearly to reinforce the mechanical strength and toughness of these soft materials. Various solutions have been proposed to solve the paradox of tough hydrogels since 2001, like double-network hydrogels (DN),<sup>1</sup> slide-ring hydrogels (SR),<sup>2</sup> nanocomposite hydrogels (NC),<sup>3</sup> etc. In the subsequent decade, a wide range of hydrogels with improved mechanical strength and toughness have been developed significantly based on or inspired from these robust hydrogels.<sup>4–12</sup> Among them, DN gels are the toughest synthetic hydrogels with a high modulus, even as tough as load-bearing cartilages and filled rubbers.<sup>13–15</sup> A universal molecular stent method has been developed recently to toughen any hydrogels based on this double network concept, which substantially broadens the applicability of this technology to various functional polymer systems.<sup>16</sup>

Extensive studies on the toughening mechanism of DN gels, consisting of polyelectrolyte as the first network and neutral polymer as the second network, have shown that yielding and large hysteresis appear in tensile deformation, and a large damage zone is formed at the crack tip, which effectively relieves the stress concentration and increases the resistance against the crack propagation.<sup>17–19</sup> The hysteresis behavior of

DN gels is associated with the fracture of the rigid and brittle polyelectrolyte network, which serves as *sacrificial bonds* in the toughening of DN gels.<sup>20</sup>

This *sacrificial bonds* mechanism has some common features with that of natural biological systems, such as collagen, bone, and mussel byssus cuticle,<sup>21–23</sup> which suggests that, introduction of any effective *sacrificial bonds* that yield and dissipate energy upon deformation will toughen the materials. On the basis of this assumption, the authors' group have introduced various motifs of *sacrificial bonds* into hydrogels.<sup>24–26</sup> One successful approach is to use densely cross-linked microgels as *sacrificial bonds* to replace the densely cross-linked polyelectrolyte macro-network for conventional DN hydrogels.<sup>25,26</sup> Our previous studies have shown that the strength and toughness of sparsely cross-linked neutral polyacrylamide (PAAm) hydrogels containing densely cross-linked polyelectrolyte microgels of poly(2-acrylamido-2-methylpropanesulfonic sodium) (PNaAMPS) is comparable to the conventional bulk DN gels at their optimal formulation, where the volume fraction of PNaAMPS microgels and the molar ratio of the PAAm to the

Received: September 14, 2012

Revised: November 14, 2012

Published: November 19, 2012

PNaAMPS in the microgel phase are two critical parameters.<sup>27</sup> These hydrogels, named as microgel-reinforced hydrogels (MR gels), can be regarded as a two-phase composite, where the disperse phase is the *rigid* double-network (DN) microgels, and the continuous phase is the *soft* PAAm matrix. We have preliminarily demonstrated that the high mechanical strength and toughness of MR gels is due to the fracture of PNaAMPS network in microgels, similar to the fracture mechanism of DN gels. However, one may not intuitively accept that the dispersed rigid phase will break first before the rupture of the soft continuous phase since the load is applied on the soft phase from the beginning of deformation. How the load transfers from the soft continuous phase to the rigid disperse phase to cause its rupture is unknown.

In this work, we make a comparison in hysteresis behavior between DN gels and MR gels, in terms of modulus and dissipated energy. Through monitoring the morphology change of the embedded microgels in MR gels during the real-time stretching process, we compare the fracture efficiency of covalent carbon–carbon (C–C) bonds in polyelectrolyte phase between bulk DN gels and DN microgels in MR gels. Finally, we explore the origin of the difference in their fracture efficiency from the point of view of the stress concentration around the microgels in the two-phase composite MR hydrogels.

## EXPERIMENTAL SECTION

**Materials.** The monomer, 2-acrylamido-2-methylpropanesulfonic sodium (NaAMPS) (Tokyo Kasei Co., Ltd.) was used as received. The cross-linker, *N,N'*-methylenebis(acrylamide) (MBAA) (Tokyo Kasei Co., Ltd.) was recrystallized from ethanol. The monomer, acrylamide (AAm) (Junsei Chemical Co., Ltd.) was recrystallized from chloroform. The UV initiator, 2-oxoglutamic acid (OA) (Wako Pure Chemical Industries, Ltd.) was used as received. The surfactant, polyglycerol polyricinoleate (PGPR) (Danisco Co., Ltd.) was used as received. The solvent, kerosene (Wako Pure Chemical Industries, Ltd.) was used as received. The dye, Alcian Blue (Wako Pure Chemical Industries, Ltd.) was used as received. Milli-Q (18.3 MΩ) water was used in all experiments.

**Synthesis. Preparation of Microgels.** Similar to our previous work, poly(2-acrylamido-2-methylpropanesulfonic sodium) (PNaAMPS) microgels were prepared by SPG (Shirasu Porous Glass) membrane emulsification and UV polymerization.<sup>26,27</sup> First, water/oil (W/O) emulsion was prepared by high-speed mini kit equipped with a hydrophobic SPG membrane (SPG Technology Co., Ltd.). The disperse phase was an aqueous solution of 1 M NaAMPS containing 4 mol % cross-linker MBAA and 0.1 mol % UV initiator OA, with respect to NaAMPS monomer. The disperse phase, stored in a pressure-tight vessel, was pressed into the continuous phase, kerosene containing 1 wt % surfactant PGPR, through the hydrophobic SPG membrane (pore diameter = 4.9 μm) under argon transmembrane pressure of 14 kPa. After being bubbled with argon for 1 h, the W/O emulsion was irradiated at 365 nm UV with intensity of 4 mW/cm<sup>2</sup> under an argon atmosphere for 8 h to get polymerized microgels. To purify the PNaAMPS microgels, they were precipitated with acetone to remove the surfactant, then reswollen in deionized water to remove the residual monomers, and finally separated by ultracentrifugation at 10<sup>4</sup> rpm for 3 times. After freeze-drying, the dried PNaAMPS microgels were obtained as fine powders.

**Preparation of MR Hydrogels.** The procedure for preparing MR hydrogels was described as our previous work.<sup>26,27</sup> 0.07 g of dried PNaAMPS microgel powders were swollen in 1 mL of the first aqueous precursor solution containing 2 M AAm, 0.01 mol % MBAA, 0.01 mol % OA, and 4 M sodium chloride (NaCl); here mol % was related to AAm monomer concentration. The NaCl was used to control the solution at a suitable operating viscosity. After equilibrium swelling, the paste-like solution was poured into a mold consisting of a

100 μm silicone spacer sandwiched by two parallel glass plates and then polymerized under an argon atmosphere with UV irradiation for 8 h. The as-prepared hydrogels were desalinated completely in deionized water and were denoted as sMR hydrogels for their single PAAm network structure. Then the sMR gels were swollen in the second aqueous precursor solution of 4 M AAm containing 0.01 mol % MBAA and 0.01 mol % OA. After equilibrium swelling, the sMR gels were covered by two parallel glass plates and wrapped by plastic film and then irradiated with UV under an argon atmosphere for 8 h. Finally, the gels were swollen in deionized water to remove the residual chemicals, and the tough MR gels with two interpenetrating PAAm networks were obtained. As a reference, a pure PAAm gel without adding any microgels was also prepared by the two-step sequential polymerization as above.

**Preparation of DN Hydrogels.** DN hydrogel films were prepared as the method described in our previous work.<sup>28</sup> With the same composition as the NaAMPS solution for synthesizing PNaAMPS microgels, an aqueous solution of 1 M NaAMPS monomer containing 4 mol % MBAA and 0.1 mol % OA was poured into a mold consisting of a 100 μm silicone spacer sandwiched by two parallel glass plates and then polymerized with UV lamps for 8 h to obtain PNaAMPS gels. The PNaAMPS gels were swollen in the first aqueous solution of 2 M AAm containing 0.01 mol % MBAA, 0.01 mol % OA, and 4 M NaCl. Here the presence of NaCl prevented the PNaAMPS gels from dramatic swelling to facilitate the operation. Then the partial-swollen PNaAMPS gels were polymerized with UV lamps for 8 h. These prereinforced gels with a single PAAm network were desalinated completely in deionized water, and then swollen to equilibrium in the second aqueous solution of 4 M AAm containing 0.01 mol % MBAA and 0.01 mol % OA, finally polymerized with UV lamps for 8 h. After equilibrium swelling, tough DN gels were obtained.

We assume that the DN gels thus prepared possessed the similar chemical composition and structure to the microgels embedded in MR gels (DN microgels). Accordingly, we could compare their mechanical behaviors.

**Characterizations. Tensile Test.** Tensile test was performed with a commercial test machine (Tensilon RTC-1150A, Orientec Co.). Fully swollen samples were cut into a dumbbell shape as standardized JIS-K6251-7 sizes (length 35 mm, width 2 mm, gauge length 12 mm) with a gel cutting machine (DumbBell Co., Ltd.). Both ends of the dumbbell-shaped samples were clamped and stretched at a constant velocity of 100 mm/min, by which the stress-strain curves were recorded.

In tensile hysteresis measurement, the samples were first elongated to a maximum strain  $\epsilon_{\text{first}}$  and then unloaded. After returning to the original point, they were reloaded and elongated immediately to an increasing maximum strain  $\epsilon_{\text{second}}$  and unloaded. The operations were carried out to  $\epsilon_{\text{third}}$ ,  $\epsilon_{\text{fourth}}$  ...,  $\epsilon_{\text{nth}}$  in the same way until the breaking point of the samples was achieved. In general, a hysteresis loop consists of a loading curve and an unloading curve after one cycle. In the case of DN and MR gels, the  $\text{nth}$  unloading curve is always overlapped by the  $n + 1$ th loading curve below  $\epsilon_{\text{nth}}$ .<sup>17,18,26</sup> Thus, we did not show the unloading curves in the hysteresis measurement for clarity. The elastic modulus  $E$  corresponding to  $\epsilon_{\text{nth}}$  is calculated from the  $n + 1$ th loading curve within the initial linear region (less than 20% strain). The dissipated energy  $\Delta U_{\text{hys}}$  of the  $\text{nth}$  hysteresis measurement for an increment of the maximum strain  $\Delta \epsilon = \epsilon_{\text{nth}} - \epsilon_{\text{n-1th}}$  is the area encompassed by the  $\text{nth}$  loading curve and the  $n + 1$ th loading curve below  $\epsilon_{\text{nth}}$ ,

$$\Delta U_{\text{hys}} = \int_0^{\epsilon_{\text{nth}}} \sigma_{\text{nth}} \, d\epsilon - \int_0^{\epsilon_{\text{nth}}} \sigma_{n+1\text{th}} \, d\epsilon \quad (1)$$

and the cumulative dissipated energy  $U_{\text{hys}}$  corresponding to  $\epsilon_{\text{nth}}$  is

$$U_{\text{hys}} = \sum_{i=1}^n \Delta U_{\text{hys}} = \sum_{i=1}^n \left( \int_0^{\epsilon_{\text{ith}}} \sigma_{\text{ith}} \, d\epsilon - \int_0^{\epsilon_{\text{ith}}} \sigma_{i+1\text{th}} \, d\epsilon \right) \quad (2)$$

**Selective Dyeing of MR Gels.** To visualize the microgels embedded in the MR gels, the MR gels were immersed in 3 vol % acetic acid aqueous solution containing 1 wt % Alcian Blue for 15 min and then

washed in deionized water. The appearance of the dyed MR gels is shown in Figure 1a. The tetravalent cationic Alcian Blue dyes the

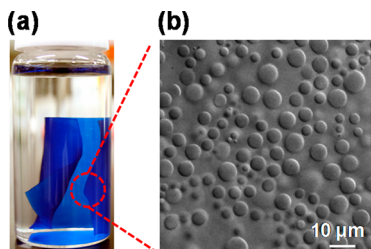


**Figure 1.** (a) Photo of dyed MR gels. (b) DIC optical micrograph of DN microgels in fully swollen MR gels.

anionic PNaAMPS microgels selectively, but not the neutral PAAm matrix, which produces a sharp contrast between the microgel phase and the matrix phase in favor of the observation of microgels under an optical microscope.

**Size Distribution of Microgels.** To characterize the size distribution of the DN microgels in MR gels, their micrographs were captured under the differential interference contrast microscope (DIC; Olympus BX50), and were analyzed by analysis software, Image-Pro Plus. Figure 1b shows a typical image. The size distribution of the microgels was determined by statistically measuring the diameter of 300 microgels. The mean diameter  $D_m$  was 6.67 μm. The coefficient of variation CV, defined as  $CV = (SD/D_m) \times 100\%$ , was ~26.3%, where SD is the standard deviation of  $D_m$ .

**Volume Fraction of Microgels.** For the traditional rubber/carbon black composites,<sup>29</sup> as well as the poly(dimethylacrylamide)/silica hybrid hydrogels,<sup>8</sup> the volume fraction of the solid fillers can be estimated easily from their formulations in feed. However, in the system of MR gels, we could not estimate the volume fraction of the microgels from the weight of the dry microgel powders added to the precursor solutions, considering the swelling of the microgel phase and the matrix phase, as well as the two-step polymerization process. Consequently, we attempted to estimate the volume fraction  $\phi_1$  of microgels from the two-dimensional DIC images of the samples by image analysis.<sup>27</sup> The total cross-section area  $A_t$  and area fraction  $\phi_s$  of microgels in one DIC image of size  $L \times L$  are estimated as

$$A_t = \pi \sum_{i=1}^n R_i^2 \quad (3)$$

$$\phi_s = \frac{A_t}{L^2} \quad (4)$$

Here,  $n$  is the number of microgels in the image area  $L \times L$ , and  $R_i$  is the radius of the  $i$ th microgel. We counted all the microgels located in the same observation plane that showed a distinct outline in Figure 1b, and ignored those with a blurred outline. The resulted error should be tolerant, because the number of the blurred microgels is small as a result of the shallow depth of the images in focus using the 100× objective lens. Assuming all the microgels with the same radius uniformly distributed spatially, the volume fraction  $\phi_1$  can be derived as

$$\phi_1 = \frac{4}{3\sqrt{\pi}} \phi_s^{3/2} \quad (5)$$

**Local Strain of Microgels.** The local deformation of the microgels embedded in MR gels was observed in *real-time* during the tensile process, utilizing the dyed MR gels under the polarizing optical microscope (POM). The spherical microgels deformed to approximate ellipsoid along the stretching direction. It is difficult to analyze the local strain of a microgel directly and exactly for several reasons: (1) we could not locate the same microgel before and after its deformation; (2) we also could not exclude the possibility of the microgel size change after or during deformation as the characteristic diffusion time of solvent in the microgel is in the order of seconds; (3) we found that the shape of microgels is not homogeneous but changes from ellipsoid to spindle-like and then to an elongated one, with the increase in the global strain  $\varepsilon$ ; (4) we observed that the deformation of the microgels has a slight size-dependence. In order to characterize the local deformation of the DN microgels, we assume that the microgels have ellipsoid shape and estimate the local strain of the microgels as follows.

$$\varepsilon_1 = \frac{c}{d} - 1 = \sqrt[3]{\left(\frac{c}{a}\right)^2} - 1 \quad (6)$$

where  $c$  and  $a$  were the major axis and the minor axis of the ellipsoid, respectively, and  $d$  is the diameter of an equivalent sphere having the same volume as the ellipsoid, estimated by the following relationship.

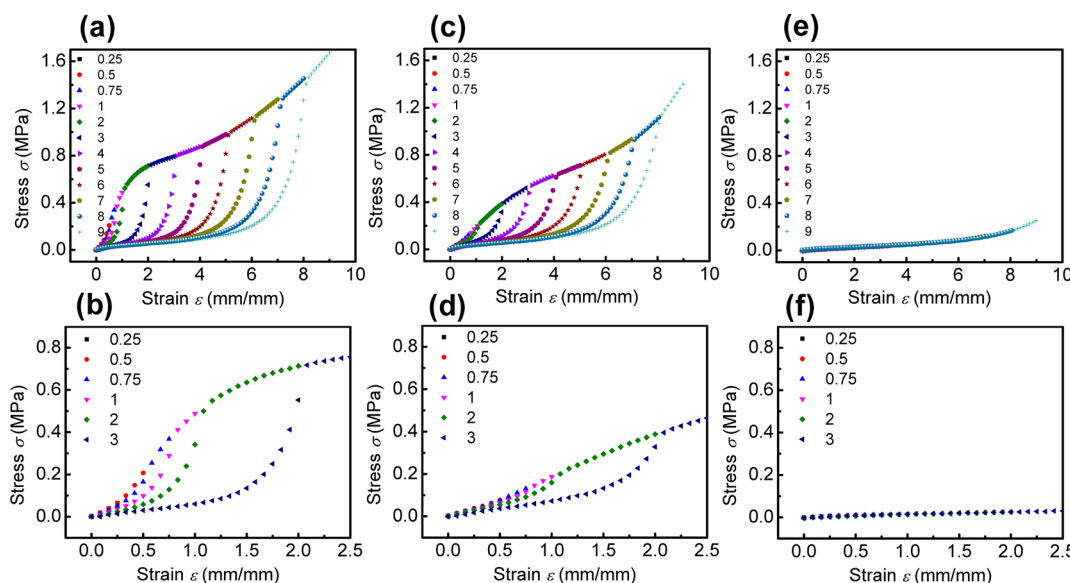


**Figure 2.** Tensile hysteresis behaviors of DN gels (a), MR gels (c), and PAAm gels (e) and the partial enlarged views ( $0 < \varepsilon < 2.5$ ) of DN gels (b), MR gels (d), and PAAm gels (f). The hysteresis measurements were repeated as the increasing level of the maximum strain  $\varepsilon$  at an increment  $\Delta\varepsilon = 0.25$  or 1. The numbers shown in the legends are the maximum strain applied for each cycle.

$$d = \sqrt[3]{a^2 c} \quad (7)$$

The  $\varepsilon_1$  thus obtained excludes the effect of possible size change caused by the deformation of the microgels. Each  $\varepsilon_1$  value was the average of five microgels with a distinct outline.

## RESULTS AND DISCUSSION

Although DN gels and MR gels own significantly different network topologies, i.e. bicontinuous structure for DN gels and two-phase composite structure for MR gels, both of them show the large hysteresis loops as shown in Figure 2a–d. The hysteresis behavior of the MR gels is irreversible, similar to that of the DN gels, indicating that permanent structure change also occurs in the MR gels. In contrast, no hysteresis phenomenon occurs for PAAm gels, even up to a strain as large as 800%, indicating no structure change (Figure 2e, f). The latter also implies that in the observed experimental condition, the PAAm gels behave as a pure elastic material and the viscous dissipative mechanism is negligible. These results demonstrate that the permanent structure change in MR gels is also due to the fracture of the polyelectrolyte network in the microgel phase, the same as the DN gels.

As shown in Figure 3, similar to the DN gels, the *initial* modulus  $E$  of MR gels at small strain also decrease

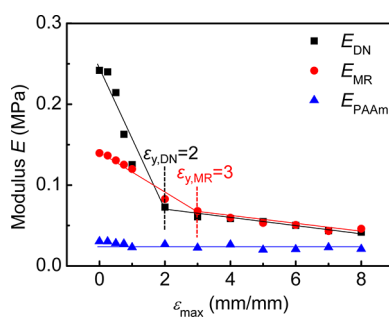


**Figure 3.** Dependence of modulus  $E$  on the maximum strain the sample experienced,  $\varepsilon_{\max}$ , for DN gels, MR gels, and PAAm gels.  $E$  was measured from the hysteresis measurements in Figure 2. The solid lines are guides to the eye for the variation of  $E$  with  $\varepsilon_{\max}$ . The obvious turning point at  $\varepsilon = 2$  for DN gels and at  $\varepsilon = 3$  for MR gels are considered as their yield strain, indicated as  $\varepsilon_{y,DN} = 2$  and  $\varepsilon_{y,MR} = 3$ , respectively.

monotonously with the maximum strain that the sample experienced,  $\varepsilon_{\max}$ , due to the persistent internal structural fracture in MR gels. The turning point at  $\varepsilon = 2$  for DN gels and at  $\varepsilon = 3$  for MR gels can be considered as the yield strain of DN gels ( $\varepsilon_{y,DN} = 2$ ) and MR gels ( $\varepsilon_{y,MR} = 3$ ), respectively.  $E$  of DN gels decreases abruptly below the yield point ( $\varepsilon < 2$ ), indicating the fast fracture in the elastic load-bearing strands of the rigid and brittle PNaAMPS network, and decreases slowly above the yield point ( $\varepsilon > 2$ ), indicating that the PNaAMPS network is less responsible for the modulus above the yield point. Similarly,  $E$  of MR gels decreases fast when  $\varepsilon < 3$  and tends to reach a constant when  $\varepsilon > 3$ . Therefore, the decreased  $E$  of MR gels suggests the rupture of covalent bonds in the microgel phase. With the increase in  $\varepsilon_{\max}$ , both DN gels and MR gels tend to reach the same constant in  $E$ , approaching the modulus of pure PAAm gels, which demonstrate that the PNaAMPS network in both DN gels and the PNaAMPS microgels in MR gels fracture significantly upon elongation and are no longer responsible for  $E$  finally.

Because the microgels are distributed in MR gels as the disperse phase, they do not carry the applied stress directly. The stress is transmitted to the microgels through the continuous PAAm matrix by chain entanglements between the microgels and the PAAm matrix. At first sight, it seems to be counterintuitive that the DN microgel phase, which is rigid and tough, fractures ahead of the soft PAAm matrix phase. However, this can be understood if we carefully look at the specific structural condition of the MR gels. As elucidated in our previous work,<sup>26,27</sup> similar to bulk DN gels, the molar ratio of the PAAm to the PNaAMPS in the microgels, which has a DN gel structure, is the most critical parameter and should reach the optimal value of 20–30 for obtaining the MR gels with the high mechanical strength and toughness. This suggests that DN gels and MR gels should have the similar fracture mechanism. When the soft matrix phase has a high concentration of PAAm strands so that its fracture stress exceeds the yield stress of the DN microgel phase, the PNaAMPS network in the microgels fractures first. This dissipates energy and softens the MR gels to avoid catastrophic failure. Thus, we conclude that the high mechanical strength and toughness of MR gels root in the sacrificial bonds of the polyelectrolyte microgels that fracture during elongation, the same as the bulk DN gels.

Owing to the absence of the viscous dissipation mechanism during the fracture process of DN and MR gels, the irreversible hysteresis (Figure 2) can be directly related to the covalent bond rupture of the polyelectrolyte phase for both DN and MR gels. In terms of energy dissipation for breaking one polymer strand, Lake and Thomas claimed that the fracture energy is amplified by the numbers of bonds per network strand, because all the bonds in one stretched strand have to be activated simultaneously even though only one bond ultimately ruptures.<sup>30</sup> In other words, the failed bonds in one strand relating to energy dissipation include one truly ruptured bond and the other unloaded ones. Assuming that Lake–Thomas theory applies to all broken loading-bearing strands in DN and MR gels, we can estimate the fraction  $\phi_b$  of covalent carbon–carbon (C–C) bonds that actually ruptured and unloaded by the fracture process according to<sup>18</sup>

$$\phi_{b,DN} = \frac{U_{hys,DN}}{C_{C-C} U_{C-C}} \quad (8)$$

$$\phi_{b,MR} = \frac{U_{hys,MR}}{\phi_1 C_{C-C} U_{C-C}} \quad (9)$$

where  $U_{hys}$  is the dissipated energy measured in the hysteresis test,  $C_{C-C}$  (139 mol/m<sup>3</sup>) is the molar concentration of C–C bonds of the polyelectrolyte phase (including the contribution of cross-linker MBAA), estimated from its volume ratio of the fully swollen state in MR gels to the as-prepared state,<sup>27</sup>  $U_{C-C}$  (360 kJ/mol) is the bond energy of a C–C bond in the carbon backbone, and  $\phi_1$  (18%) is the volume fraction of microgels in MR gels, estimated from Figure 1b by eq 5.

The dissipated energy for a unit-strain increment,  $\Delta U_{hys}$ , and cumulative dissipated energy,  $U_{hys}$ , can be calculated from the encompassed area of the hysteresis cycle by eqs 1 and 2, as shown in Figure 4a,b. DN gels show the larger  $\Delta U_{hys}$  and  $U_{hys}$  than MR gels, which should be attributed to a larger amount of C–C bonds in DN gels. In fact, if we take into the consideration of the microgel volume fraction  $\phi_1$ , MR gels show higher values of  $\Delta\phi_b$  and  $\phi_b$  than those of DN gels at the

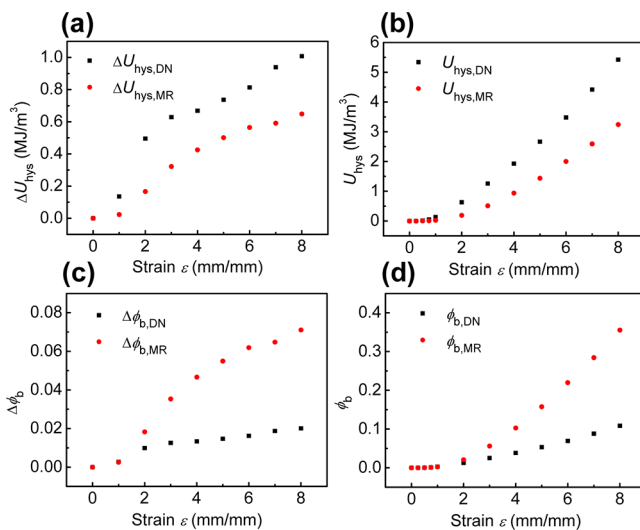


**Figure 4.** Dependences of (a) dissipated energy for a unit-strain increment  $\Delta U_{\text{hys}}$ , (b) cumulative dissipated energy  $U_{\text{hys}}$ , (c) fraction of broken C–C bonds for a unit-strain increment  $\Delta \phi_b$ , and (d) cumulative fraction of broken C–C bonds  $\phi_b$ , on the maximum strain  $\epsilon$  for DN gels and MR gels.

same strain  $\epsilon$  (Figure 4c, d). As shown in Figure 4c, the PNaAMPS network in DN gels fractures fast in the initial region ( $0 < \epsilon < 2$ ), and fractures steadily in the yielding and hardening region ( $\epsilon > 2$ ). The PNaAMPS microgels in MR gels show little fracture in the initial region ( $0 < \epsilon < 1$ ), and fracture fast in the intermediate region ( $1 < \epsilon < 3$ ), finally fracture slowly in the large deformation region and hardening region ( $\epsilon > 3$ ). In Figure 4d, we find both  $\phi_b$  of DN gels and MR gels are almost constant in the range  $0 < \epsilon < 1$ , and increase linearly when  $\epsilon > 1$ , which means C–C bonds fracture few when  $0 < \epsilon < 1$ , and fracture persistently when  $\epsilon > 1$ . At  $\epsilon = 8$ ,  $\phi_b$  of MR gels reaches 36%, three times of the DN gels that is only 11%, which indicates the higher fracture efficiency of MR gels than that of DN gels.

According to Figure 3,  $\epsilon = 2$  and  $\epsilon = 3$  can be regarded as the yield point for DN gels and MR gels, respectively.  $E$  of DN and MR gels show notable changes below and above their yield point. Most modulus-related load-bearing strands rupture until the yield point, but the corresponding values of  $\phi_b$  at the yield

point are only 1% and 6% for DN gels and MR gels, respectively. These so small values of  $\phi_b$  still have a significant impact on  $E$ , which reveal rather heterogeneous structure in both the PNaAMPS network of DN gels and the PNaAMPS microgels of MR gels.<sup>18,31</sup> The heterogeneous structure of DN gels will be discussed in detail in a separate paper.<sup>32</sup>

Figure 4d shows that MR gels have the higher fracture efficiency than DN gels at the same global strain  $\epsilon$ . To further compare the fracture efficiency between DN microgels in MR gels and bulk DN gels, we perform the real-time optical observation of MR gels at different tensile strains  $\epsilon$ , and correlate the local strain of microgels  $\epsilon_1$  defined in eq 6 with the global strain of MR gels  $\epsilon$  (Figure 5). Below the yield point ( $0 < \epsilon < 3$ , Figure 5a–c), the microgels show a much smaller  $\epsilon_1$  than the applied global strain  $\epsilon$  on MR gels, which indicates that the microgels own the higher modulus than the PAAm matrix to resist uniaxial deformation. Above the yield point ( $\epsilon > 3$ , Figure 5d–f), the microgels deform with a high degree, demonstrating a softening of the microgels; the background color, relating to the uniaxial orientation of the PAAm matrix, emerges with a sharper contrast in comparison to that below the yield point, which indicates the occurrence of the large deformation of the PAAm matrix.

Figure 5g shows the quantitative relation between  $\epsilon_1$  and  $\epsilon$ , where  $\epsilon_1$  has two distinct regions with a boundary at the yield point ( $\epsilon = 3$ ). In the range  $0 < \epsilon < 3$ ,  $\epsilon_1$  increases slightly with  $\epsilon$ , with a small slope of 0.2; when  $\epsilon > 3$ ,  $\epsilon_1$  increases sharply with  $\epsilon$ , with a large slope of 1.18. On the basis of the smaller  $\epsilon_1$  of the microgels below the yield point, we have demonstrated that isostress model is applicable to MR gels in the small deformation region.<sup>27</sup> With the increase of the strain, the stress increases and at the  $\epsilon$  of 3, the load-bearing strands of the PNaAMPS network in the microgel phase fracture significantly and the microgels start to yield, according to the  $E$  dependence of MR gels on  $\epsilon$  as shown in Figure 3, which leads to the extensive extension of the soft PAAm strands entrapped in the microgel phase. In other words, the yield of the incorporated microgels dominates the large deformation of MR gels. If we extrapolate the fitting line of  $\epsilon_1 = 1.18\epsilon - 2.86$  to cross the line of  $\epsilon_1 = \epsilon$ , the intersection point shows a  $\epsilon$  of 16, at which the PNaAMPS network in the microgel phase will fracture into a level that it no longer plays any role as physical cross-linker, and the MR gels will approach the pure PAAm gels.

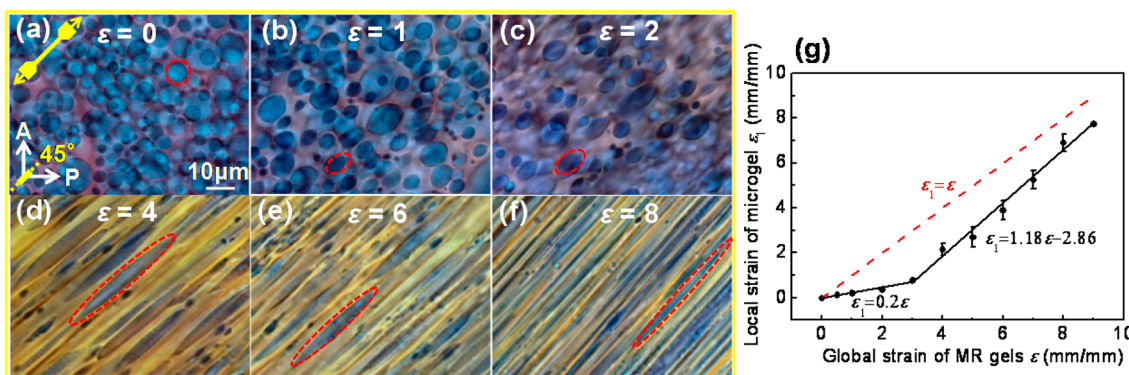


**Figure 5.** (a–f) Real-time optical observation of MR gels at different tensile strains  $\epsilon$  under the polarizing optical microscope (POM), equipped with the crossed polarizers and the 530 nm tint plate. The microgels were selectively dyed by the Alcian Blue. The sample was stretched 45° against the polarizers. The red dashed circles indicate the deformed microgels. (g) Average local strain of microgels  $\epsilon_1$  as a function of the global strain of MR gels  $\epsilon$ . The black solid lines are the linear fits for two regions of  $0 < \epsilon < 3$  and  $3 < \epsilon < 7$ , respectively, and the red dashed line indicates the case of  $\epsilon_1 = \epsilon$ , that the microgel phase and the matrix phase deform with the same extent. Each  $\epsilon_1$  is the statistic average of 5 microgels with a distinct outline.

Accordingly, although the macroscopic yielding phenomenon of MR gels is not as distinct as that of conventional DN gels,<sup>17,20</sup> in essence, similar PNaAMPS network rupture process occurs at the large deformation for the MR gels as that of DN gels, where the flexible PAAm network transforms the conformation from random coil to stretching-induced uniaxial orientation and hardening.

As the true strain applied on the DN microgel phase,  $\varepsilon_1$ , is different from the global value,  $\varepsilon$ , we replot Figure 4d as a function of the true strain using the result of Figure 5g. Figure 6

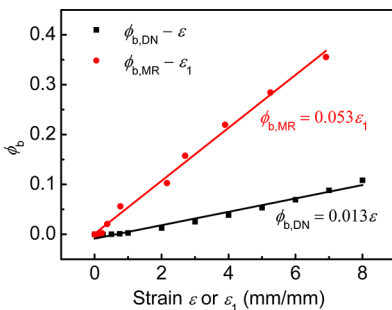


**Figure 6.** Comparison of the cumulative fraction of broken C–C bonds  $\phi_b$  between bulk DN gels and DN microgels in MR gels. The solid lines are the linear fits for bulk DN gels and DN microgels, respectively.

reflects the fracture efficiency of C–C bonds for bulk DN gels and DN microgels in the MR gels against the true strain of their DN phase. The latter shows higher fracture efficiency than the former at the same strain. Dividing the slope of the fitting line of DN microgels by that of DN gels, we find that the fracture efficiency of DN microgels is four times higher than that of DN gels at the same strain.

One plausible interpretation for this interesting finding is the stress concentration around the microgels. As shown in Figure 3 and Figure 5g, the yield strain of DN gels and MR gels is  $\varepsilon_{y,DN} = 2$  and  $\varepsilon_{y,MR} = 3$ , respectively, corresponding to the yield stress of  $\sigma_{y,DN} = 0.71$  MPa and  $\sigma_{y,MR} = 0.53$  MPa based in Figure 2. As the true yield stress of DN microgels should equal to that of bulk DN gels, the relation of  $\sigma_{y,DN} > \sigma_{y,MR}$  indicates the stress concentration around the DN microgels. Quantitatively, the stress concentration factor for MR gels  $K$ , defined as  $K = \sigma_{y,DN}/\sigma_{y,MR}$ , is 1.34. As a fact, this stress concentration effect is clearly visualized in Figure 7a, where the DN microgels deformed into spindle-like shape at yielding ( $\varepsilon = 3$ ). This indicates that the yielding occurred preferentially at the two poles along the tensile direction. Figure 7b illustrates the structure of the spindle-like DN microgel under uniaxial tension. At the initial state of elongation, the soft PAAm matrix deforms with a larger strain, due to its lower modulus than that of DN microgels; in contrast, the DN microgels exhibit a smaller strain as ellipsoidal shape (as shown in Figure 5b). With the increase in the applied external stress, the modulus of the PAAm matrix induced by stretching increases dramatically (strain hardening) and exceeds that of the DN microgels, at which point the two poles of the DN microgels cannot sustain the exerted stress and start to yield, resulting in the spindle-like shape of the DN microgels. Highly cross-linked PNaAMPS network in these yield regions fracture substantially to facilitate the orientation of the coiled PAAm strands to resist stress, meanwhile, substantial amount of energy dissipates upon the rupture of the PNaAMPS network. The boundary between the ruptured and intact regions, as

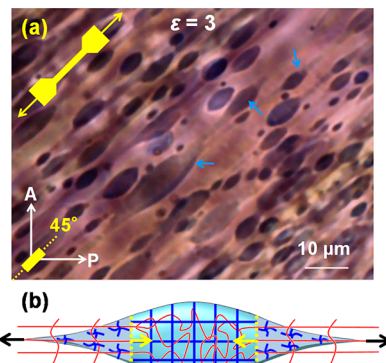


**Figure 7.** (a) Real-time optical observation of MR gels at the yield point of  $\varepsilon = 3$  under the POM. The microgels deformed the shape from sphere to spindle that are highlighted by the blue arrows. The test conditions are the same as shown in Figure 5. (b) Schematic illustration of a spindle-like DN microgel under uniaxial tension. Because of the stress concentration, the two poles of the microgel yield first under deformation, in which the brittle short chains (blue) rupture, and then the rupture advances toward the equator with further deformation. The ductile long chains (red) are highly elongated at the two poles where the short chains have ruptured. The yellow dashed lines indicate the boundary between ruptured and intact brittle network, and the yellow arrows indicate the boundary advancing direction.

indicated by the yellow dashed lines in Figure 7b, advances toward the equator of the microgels. During the whole yielding process, a slight increase in stress gives rise to a large strain due to the stretching-induced orientation of the PAAm strands entrapped in the DN microgels, which is also well verified by Figure 2c. Consequently the higher fracture efficiency of DN microgels than bulk DN gels stems from the stress concentration around the microgels, which leads to the preferential yielding at the two poles of the spherical DN microgels.

It is well-known that in a composite system, stress concentration occurs at the interface between inclusion and matrix due to mismatching in modulus. As the extreme case, for an absolute rigid spherical inclusion in an infinite matrix under uniaxial tension ( $E_{inclusion}/E_{matrix} = \infty$ ), Goodier derives the maximum stress concentration factor  $K$  at the two poles of the inclusion as<sup>33</sup>

$$K = \frac{2}{1 + \nu} + \frac{1}{4 - 5\nu} \quad (10)$$

Here  $\nu$  is the Poisson's ratio of the matrix. In the range of  $0 \leq \nu \leq 0.5$ , eq 10 gives an almost invariable  $K$  belonging to the range of  $1.93 \leq K \leq 2.25$ . The stress concentration around the DN microgels can also be attributed to the mismatching in the modulus of the rigid DN microgels with the soft matrix phase. Our observation of a stress concentration factor  $K = 1.34$  for MR gels is in reasonable agreement with the predicted range. In addition, the possible high PAAm chain density and entanglements on the surface of the microgels, as a result of the confined swelling of the PAAm matrix, might also contribute to the stress concentration.

## CONCLUSIONS

We have synthesized a kind of strong and tough MR hydrogels with a novel two-phase composite structure, where the disperse phase is viewed as the rigid DN microgels, and the continuous

phase is the soft PAAm matrix. The embedded DN microgels have been visualized directly by optical microscopy, benefitting from the following three features of MR gels: (1) The microgels used is at mesoscale, with an average diameter of  $\sim 5 \mu\text{m}$ ; (2) The prepared MR gel films is quite thin, with a thickness of  $\sim 300 \mu\text{m}$ ; (3) The incorporated microgels are dyed selectively by Alcian Blue to increase the refractive index difference between the microgel phase and the matrix phase. In MR gels, the densely cross-linked PNaAMPS microgels act as multifunctional physical cross-linkers to confine the swelling of sparsely cross-linked PAAm matrix through mutual entanglement. The entanglement between the PAAm matrix phase and the microgels phase plays a crucial role in stress transmission. On the basis of the irreversible hysteresis, we conclude that the high strength and toughness of MR gels root in the irreversible rupture of the polyelectrolyte network in the DN microgels, as sacrificial bonds, similar to the fracture mechanism of DN gels. Further, we find that the DN microgels embedded in the PAAm matrix show four times higher in fracture efficiency of the sacrificial bonds than the bulk DN gels at the same strain, as a result of the stress concentration around the two poles of microgels, with a stress concentration factor of 1.34. This leads to the preferential yielding at the two poles of the spherical DN microgels at a smaller nominal stress.

Owing to the direct visualization of the embedded microgels, these strong and tough MR hydrogels will be excellent model systems for investigating fundamental issues of the fracture behavior of soft, highly deformable materials, of which our mechanistic understanding of the fracture is still much more limited.<sup>34</sup>

## AUTHOR INFORMATION

### Corresponding Author

\*E-mail: gong@mail.sci.hokudai.ac.jp.

### Notes

The authors declare no competing financial interest.

## ACKNOWLEDGMENTS

This research was financially supported by a Grant-in-Aid for Scientific Research (S) (No. 12422506) from Japan Society for the Promotion of Science (JSPS).

## REFERENCES

- (1) Gong, J. P.; Katsuyama, Y.; Kurokawa, T.; Osada, Y. *Adv. Mater.* **2003**, *15*, 1155.
- (2) Okumura, Y.; Ito, K. *Adv. Mater.* **2001**, *13*, 485.
- (3) Haraguchi, K.; Takehisa, T. *Adv. Mater.* **2002**, *14*, 1120.
- (4) Waters, D. J.; Engberg, K.; Parke-Houben, R.; Hartmann, L.; Ta, C. N.; Toney, M. F.; Frank, C. W. *Macromolecules* **2010**, *43*, 6861.
- (5) Sakai, T.; Matsunaga, T.; Yamamoto, Y.; Ito, C.; Yoshida, R.; Suzuki, S.; Sasaki, N.; Shibayama, M. *Macromolecules* **2008**, *41*, 5379.
- (6) Kaneko, T.; Tanaka, S.; Ogura, A.; Akashi, M. *Macromolecules* **2005**, *38*, 4861.
- (7) Huang, T.; Xu, H. G.; Jiao, K. X.; Zhu, L. P.; Brown, H. R.; Wang, H. L. *Adv. Mater.* **2007**, *19*, 1622.
- (8) Lin, W. C.; Fan, W.; Marcellan, A.; Hourdet, D.; Creton, C. *Macromolecules* **2010**, *43*, 2554.
- (9) Henderson, K. J.; Zhou, T. C.; Otim, K. J.; Shull, K. R. *Macromolecules* **2010**, *43*, 6193.
- (10) Wang, Q.; Mynar, J.; Yoshida, M.; Lee, E.; Lee, M.; Okuro, K.; Kinbara, K.; Aida, T. *Nature* **2010**, *463*, 339.
- (11) Haque, M. A.; Kamita, G.; Kurokawa, T.; Tsujii, K.; Gong, J. P. *Adv. Mater.* **2010**, *22*, 5110.
- (12) Sun, J. Y.; Zhao, X.; Illeperuma, W. R. K.; Chaudhuri, O.; Oh, K. H.; Mooney, D. J.; Vlassak, J. J.; Suo, Z. *Nature* **2012**, *489*, 133.
- (13) Fung, Y. C. *Biomechanics: Mechanical properties of living tissues*, 2nd ed.; Springer-Verlag: New York, 1993.
- (14) Taylor, D.; O'Mara, N.; Ryan, E.; Takaza, M.; Simms, C. *J. Mech. Behav. Biomed. Mater.* **2012**, *6*, 139.
- (15) Naficy, S.; Brown, H. R.; Razal, J. M.; Spinks, G. M.; Whitten, P. G. *Aust. J. Chem.* **2011**, *64*, 1007.
- (16) Nakajima, T.; Sato, H.; Zhao, Y.; Kawahara, S.; Kurokawa, T.; Sugahara, K.; Gong, J. P. *Adv. Funct. Mater.* **2012**, *22*, 4426.
- (17) Na, Y.-H.; Tanaka, Y.; Kawauchi, Y.; Furukawa, H.; Sumiyoshi, T.; Gong, J. P.; Osada, Y. *Macromolecules* **2006**, *39*, 4641.
- (18) Webber, R. E.; Creton, C.; Brown, H. R.; Gong, J. P. *Macromolecules* **2007**, *40*, 2919.
- (19) Yu, Q. M.; Tanaka, Y.; Furukawa, H.; Kurokawa, T.; Gong, J. P. *Macromolecules* **2009**, *42*, 3852.
- (20) Gong, J. P. *Soft Matter* **2010**, *6*, 2583.
- (21) Thompson, J. B.; Kindt, J. H.; Drake, B.; Hansma, H. G.; Morse, D. E.; Hansma, P. K. *Nature* **2001**, *414*, 773.
- (22) Fantner, G. E.; Hassenkam, T.; Kindt, J. H.; Weaver, J. C.; Birkedal, H.; Pechenik, L.; Cutroni, J. A.; Cidade, G. A. G.; Stucky, G. D.; Morse, D. E.; Hansma, P. K. *Nat. Mater.* **2005**, *4*, 612.
- (23) Harrington, M. J.; Masic, A.; Holten-Andersen, N.; Waite, J. H.; Fratzl, P. *Science* **2010**, *328*, 216.
- (24) Haque, M. A.; Kurokawa, T.; Kamita, G.; Gong, J. P. *Macromolecules* **2011**, *44*, 8916.
- (25) Saito, J.; Furukawa, H.; Kurokawa, T.; Kuwabara, R.; Kuroda, S.; Hu, J.; Tanaka, Y.; Gong, J. P.; Kitamura, N.; Yasuda, K. *Polym. Chem.* **2011**, *2*, 575.
- (26) Hu, J.; Hiwatashi, K.; Kurokawa, T.; Liang, S. M.; Wu, Z. L.; Gong, J. P. *Macromolecules* **2011**, *44*, 7775.
- (27) Hu, J.; Kurokawa, T.; Hiwatashi, K.; Nakajima, T.; Wu, Z. L.; Liang, S. M.; Gong, J. P. *Macromolecules* **2012**, *45*, 5218.
- (28) Liang, S.; Yu, Q. M.; Yin, H.; Wu, Z. L.; Kurokawa, T.; Gong, J. P. *Chem. Commun.* **2009**, 7518.
- (29) Litvinov, V. M.; Orza, R. A.; Klüppel, M.; van Duin, M.; Magusin, P. C. M. M. *Macromolecules* **2011**, *44*, 4887.
- (30) Lake, G. J.; Thomas, A. G. *Proc. R. Soc. London, Ser. A* **1967**, *300*, 108.
- (31) Tominaga, T.; Tirumala, V. R.; Lin, E. K.; Gong, J. P.; Furukawa, H.; Osada, Y.; Wu, W. L. *Polymer* **2007**, *48*, 7449.
- (32) Nakajima, T.; Kurokawa, T.; Ahmed, S.; Wu, W.; Gong, J. P. *Soft Matter* **2012**, in press.
- (33) Goodier, J. N. *J. Appl. Mech.* **1933**, *55*, 39.
- (34) Shull, K. R. *Nature* **2012**, *489*, 36.